Electronic Supplementary Material (ESI) for Nanoscale Advances.

Supporting Information

Boosting Performance of NO_2 Gas Sensor based on *n-n* Type Mesoporous ZnO@In_2O_3 Heterojunction Nanowires: *In-situ* Conducting Probe Atomic Force Microscopic Elucidation of Room Temperature, Localized Electron Transfer

Ramakrishnan Vishnuraj[1], Karthikeyan K. Karuppanan[1], Mahaboobbatcha Aleem[1] and Biji Pullithadathil[1*]

**Corresponding author Email: bijuja123@yahoo.co.in; pbm@psgias.ac.in*

1. Characterization Techniques:

The XRD patterns were acquired using Power X-ray diffractometer (Rigaku ULTIMA IV, Japan) using Cu Kα radiation of wavelength 1.5418 Å at a scanning rate of 0.02°/ sec in the 2θ range of 20– 80°. Micro Raman spectra (WITec, 300 Alpha, Germany) of heterojunction ZnO@In_2O_3nanowires were obtained using He-Cd laser (λ = 532 nm) as an excitation light source with 1800g/mm gratings. The structure and morphology of the ZnO@In_2O_3 heterojunction nanowires were examined using High-Resolution Transmission Electron Microscopy (JEOL JEM-2010, Japan) and Scanning Electron Microscopy (ZEISS EVO 18, USA), with in-built Energy-Dispersive X-Ray Spectrometer (Oxford Instruments, INCA, UK). CaRIne crystallography 3.1 was used to simulate the lattice atoms present in each plane and calculated the ratio of $Zn^{2+}$and O^{2-} ions present in the ZnO planes and as well asIn^{3+} and O^{2-} present in the In_2O_3 planes. UV-DRS absorption spectra were acquired using JASCO UV (V-750) spectrophotometer. The spreading resistance imaging and scanning kelvin probe microscopy analysis of the prepared materials was performed on multimode scanning probe microscope (NTMDT, NTEGRA-AURA, Russia) under ambient conditions (24°C). Photoluminescence (PL) characterization was carried out using spectrofluorophotometer (RF-5301PC, Shimadzu, Japan). X-ray photoelectron spectroscopy (XPS) measurements were performed on a Phoibos 100 MCD energy analyzer using monochromatized Al Kα excitation to analyze the elemental and chemical states of the materials. AFORS-HET software v2.5 was used to simulate the energy band bending diagram of ZnO@In_2O_3 heterojunction nanowires.

Brunauer-Emmett-Teller (BET) specific surface area analysis of samples was estimated by nitrogen adsorption-desorption isotherm (BELSORP-MAX, Microtrac BEL Corp, Japan).

2. Evaluation of gas sensor sensing properties:

The sensor device was fabricated as inter-digitated array (IDA) electrode made of Au (~150 nm) with an inter finger gap of 16 μm using planar DC magnetron sputtering on alumina substrates. Thin films of porous ZnO nanowires and porous ZnO@In_2O_3 heterojunction nanowires (1mg/mL) were dispersed in ethanol and drop-casted on IDA transducer electrodes at 55^oC.The gas sensing properties of the materials were analyzed using a custom-built gas sensor test station consisting of a stainless steel double-walled test chamber equipped with temperature-controlled hot stage, sensor holder, mass flow controllers (MFC, Alicat, USA), digital multimeter (Agilent 34401A, USA) connected with a data acquisition system interfaced with Labview software. During measurements, NO_2 gas was mixed with dry nitrogen to achieve the desired concentrations and the flow rate was maintained as 300sccm using mass flow controllers (Alicat, U.S.A.). A temperature controller (Eurotherm, 2420, U.K.) was used to maintain the working temperature of the sensor mounted inside the sensing chamber. Constant gas pressure was maintained in the sensing chamber (710 Torr) throughout the testing which was measured using Baratron 722B Absolute Capacitance Manometer (MKS Instruments, Singapore).

3. Optical Band gap calculation of ZnO@In_2O_3 heterojunction nanowires using UV–visible diffuses reflectance spectroscopy (DRS):

Solid state UV–visible diffuses reflectance spectra (DRS) of ZnO nanowires and core-shell heterojunction ZnO@In_2O_3nanowires shown in **Figure S1**.ZnO nanowires exhibits UV absorption peak centered at 365nm, which corresponds to the ground excitonic peak of Zn-O. Also core-shell ZnO@In_2O_3nanowires exhibits the same with an additional broad peak near the region of 450nm. The crystalline purity of the sample has been confirmed by observing absence of additional peaks in the spectrum.

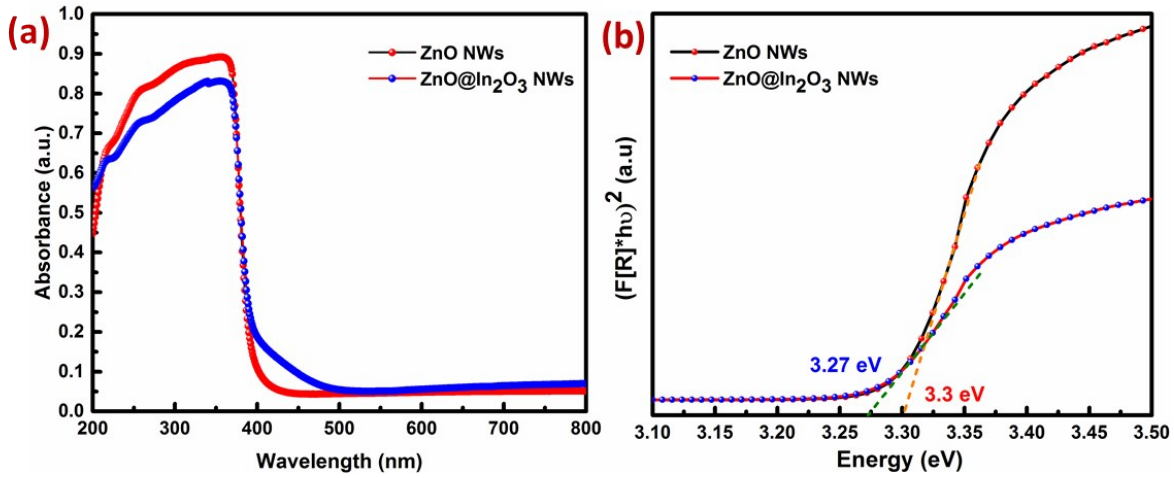

Figure S1(a) UV–Vis DRS spectra of ZnO nanowires and mesoporous ZnO@In_2O_3 heterojunction nanowires. (b) Kubelka-Munk function versus energy plots of ZnO nanowires and ZnO@In_2O_3 heterojunction nanowires.

The band gap energy of the samples is measured by the extrapolation of the linear portion of the graph between the modified Kubelka-Munk function $[F(R)*hv]^2$ versus photon energy (hν) shown in the inset **Figure S1(b)**.

$$F_{KM} = \frac{(1-R)^2}{2R} \qquad \text{(S1)}$$

The band gaps of the pristine ZnO nanowires and heterojunction ZnO@In_2O_3nanowires were calculated to be 3.3 and 3.27 eV respectively. The considerable change observed in the band gaps is due to the interfacial electron transfer between ZnO nanowires and In_2O_3nanocluster as shell layer.

4. Morphological analysis of mesoporous ZnO nanowires:

TEM analysis was carried out for ZnO nanowires to infer about the structure and morphological characteristics. Fig. S2(a) shows the TEM images of bare ZnO nanowires, where the uniform distribution of nanowires having length and width of 15 ± 0.5 µm and 150 ± 0.5 nm respectively were observed. Each nanowire extends to several micrometers with high aspect ratio as suited for electronics and sensing applications. Fig. S2 (c) showing HR-TEM image of ZnO

nanowires clearly shows the d-spacing value of 0.25 nm between the adjacent lattice planes corresponding to (100) plane lattice distance of hexagonal-wurtzitestructured ZnO,indicating the growth direction along *c*-axis [0001]. Fig. S2(b) showing the SAED pattern of ZnO nanowires clearly implies the growth direction of ZnO in c-axis with single crystalline nature. The SAED pattern were indexed and matching with the standard JCPDS data card no.65-3411.

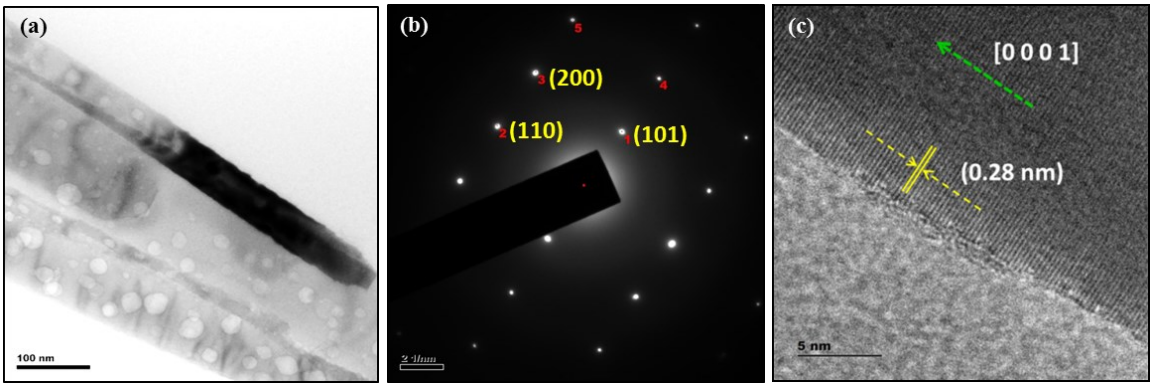

Figure S2. (a) TEM and (c) HRTEM image of ZnO nanowires and (c) corresponding SAED pattern of ZnO nanowires.

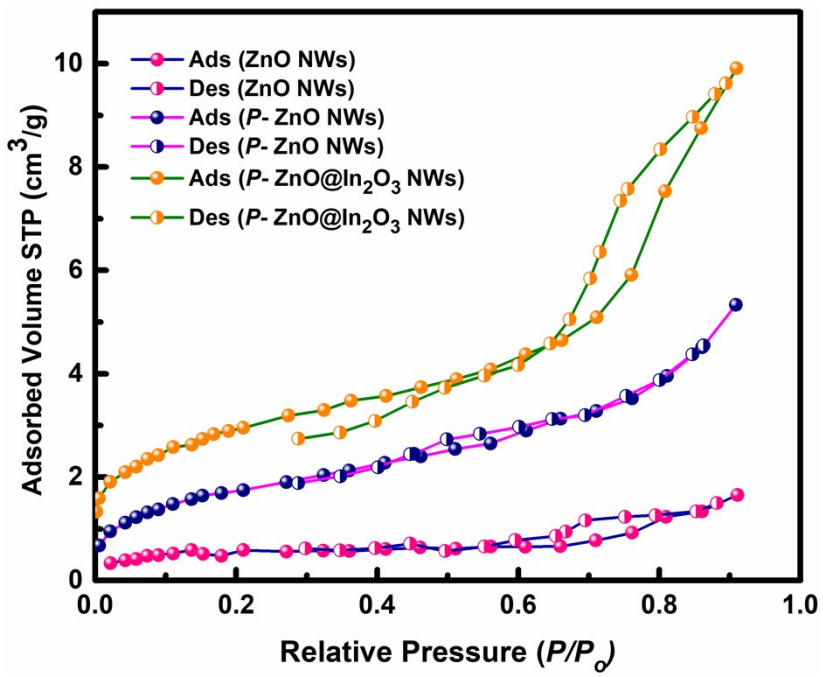

Figure S3. Typical nitrogen adsorption–desorption isotherm plots of bare ZnO, porous ZnO and porous ZnO@In_2O_3 nanowires.

Table S1. BET parameters of bare ZnO, porous ZnO and porous ZnO@In_2O_3nanowires:

Sample	Surface area (m^2/g)	Pore volume (cm^3/g)	Pore size (nm)	Pore Specific Surface Area (m^2/g)
Bare ZnO nanowires	1.8816	2.5628	3.0200	3.6655
Porous ZnO nanowires	6.2636	8.2457	3.5133	10.5092
Porous ZnO@In_2O_3 heterojunction nanowires	10.2961	15.2394	4.8705	12.5193

5. SKPM tip calibration:

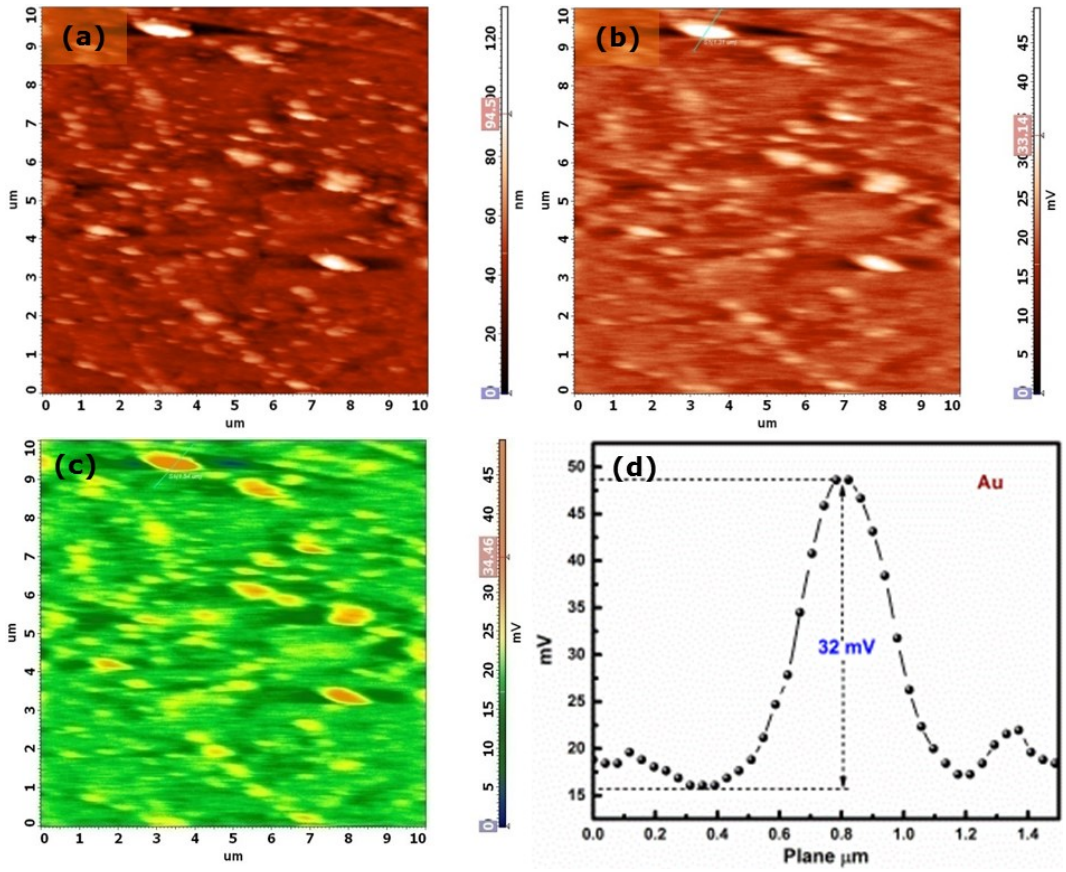

Figures S4. SKPM measurements on standard Au film for calibration of Au coated Si tip (a) topographic image of Au thin films (b-c) surface potential difference of Au thinfilms (d) CPD plot.

The work function calibration of the tip using the known value of Au film based on the above equation (5) is given below,

$$4.9\ \text{eV} - 1.096\ x\ 1.60\ x\ 10^{-19} x\ 6.24\ x\ 10^{18}\text{eV} = \varphi_{tip}$$

$$4.86805\ \text{eV} = \varphi_{tip}$$

Table: S2 NO_2 Gas sensing parameter of bare and heterojunction ZnO@In_2O_3 nanowires:

Conc. of NO_2 (ppm)	ZnO nanowires			Heterojunction ZnO@In_2O_3nanowires		
	Response [(Rg− Ra)/Ra] S (%)	Response time (s)	Recovery time (s)	Response [(Rg− Ra)/Ra] S (%)	Response time (s)	Recovery time (s)
0.5	30.79	39	76	274.1	4	76
1	121.97	26	114	722.9	6	97
1.5	186.49	26	196	799.8	10	116
2	290.55	29	166	908.7	11	128
2.5	391.10	35	239	1074.2	12	175
3	498.35	36	256	1419.9	13	189

6. NO_2 Adsorption/Desorption Kinetics of heterojunction ZnO@In_2O_3 nanowires:

The chemical adsorption kinetics of NO_2 gas on the surface of ZnO nanowires and P ZnO@In_2O_3 heterojunction nanowires was further elucidated using Elovich model. The general form of Elovich plot can be expressed as,

$$q = \frac{1}{\alpha} ln(\alpha\alpha') + \frac{1}{\alpha} ln(t) \qquad \text{(S2)}$$

Where, q is the amount of gas adsorbed during time and t, α, and α′ are constants. The change in the conductance (C_{tg}−C_0) is proportional to the amount of adsorbed NO_2 molecules (q). The constant α′ is the initial adsorption rate and α is the measure of potential barrier for successive adsorption of gas molecules, that is, depleted layer formed by previously adsorbed gas molecules

that act as a barrier for the next incoming gas molecules. The values of these constants can be obtained from the slope and the intercept by plotting ($C_{tg}-C_0$) versus ln(t). C_0 and C_{tg} are conductance of ZnO nanowires and mesoporous heterojunction ZnO@In_2O_3 nanowires at t=0 and t=g upon exposing to NO_2 gas environment, respectively.

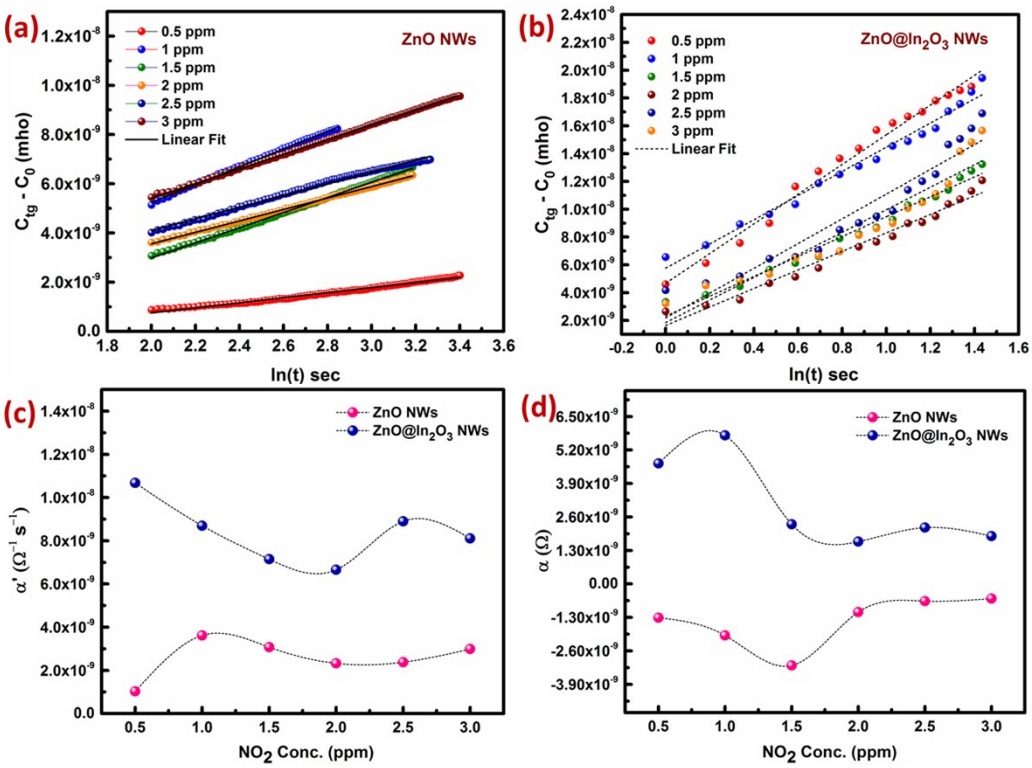

Figure S5 (a-b) Elovich plot for NO_2 adsorption on ZnO nanowires and mesoporous heterojunction ZnO@In_2O_3nanowires surfaces (c-d) Relationship between initial adsorption rate (α′), barrier potential (α) and NO_2 concentration of ZnO nanowires and heterojunction ZnO@In_2O_3nanowires.

Table:S3 Values of constants α' and α from Elovich plot:

Conc. of NO_2	Initial Adsorption rate (α') (10^{-09})Ω^{-1} s^{-1}		Surface Potential barrier (α) MΩ	
	ZnO Nanowires	ZnO@In_2O_3Nanowires	ZnO Nanowires	ZnO@In_2O_3Nanowires
0.5	0.93	10.71	4.00	19.92
1	3.92	8.70	2.53	20.40
1.5	4.24	7.15	3.46	19.79
2	3.15	6.66	1.97	20.64
2.5	3.88	8.90	4.66	19.83
3	4.02	8.11	1.05	19.44

Table: S4 Calculated parameters from the KPFM analysis:

Sample	Work Function (φ_s) eV	Band Bending (Φ_B) eV	Carrier Density (n_s) 10^{19} cm^{-2}	Depletion Width (nm)
ZnO nanowires in Air	4.83	1.927	1.29	2.96
ZnO nanowires in NO_2	4.93	1.959	1.02	3.34
ZnO@In_2O_3nanowires in Air	4.97	2.049	1.18	3.19
ZnO@In_2O_3nanowires in NO_2	5.01	2.086	0.87	3.78

7. Cross selectivity of the gases:

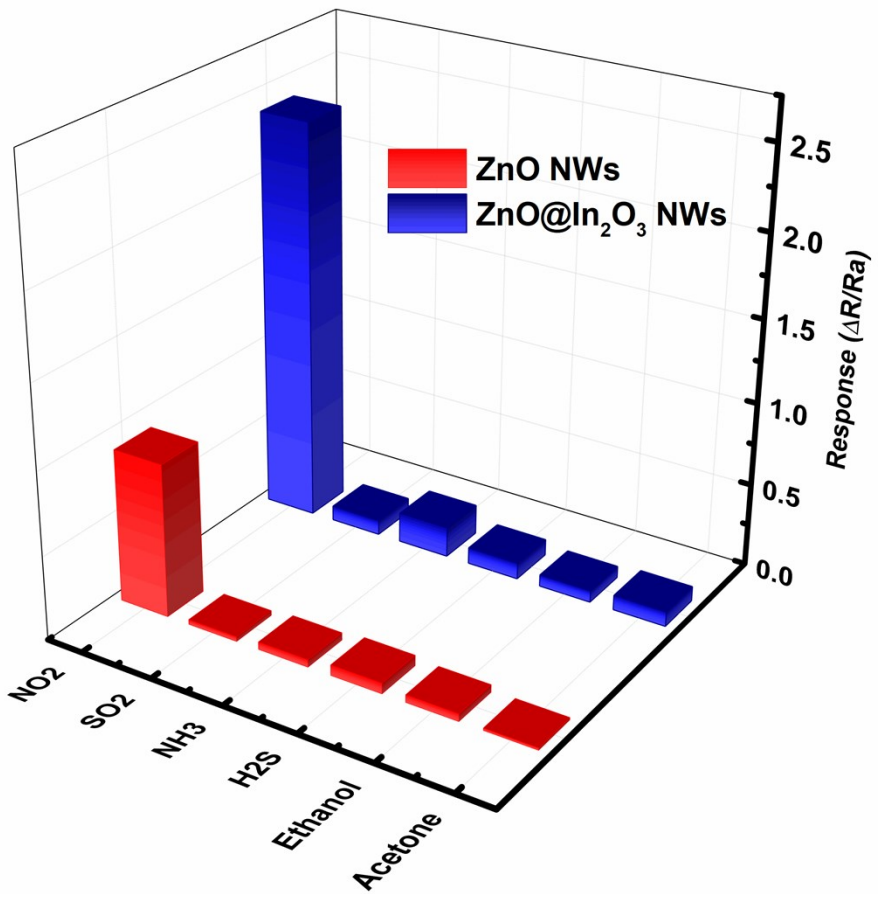

Figure S6 Cross selectivity studies of ZnO nanowires and core-shell heterojunction ZnO@In_2O_3 nanowires.

To observe the cross interference selectivity properties of the mesoporous heterojunction ZnO@In_2O_3 nanowires towards NO_2 gas, their responses were analyzed towards exposure to several interfering gases, such as NH_3, H_2S, ethanol, acetone and SO_2 by keeping constant 2 ppm gas concentration (**Figure S7**). The heterojunction material was observed to be greatly selective towards NO_2 rather than other reducing and volatile organic gases due to the presence of In_2O_3 nanocluster effectively forming heterojunction onto the surfaces of ZnO Nanowires which could enhances the physisorption process. The charge accumulated at the junction interface of In_2O_3 nanocluster favors the strong adsorption of the oxidizing gas (NO_2) than other reducing and volatile organic gases.

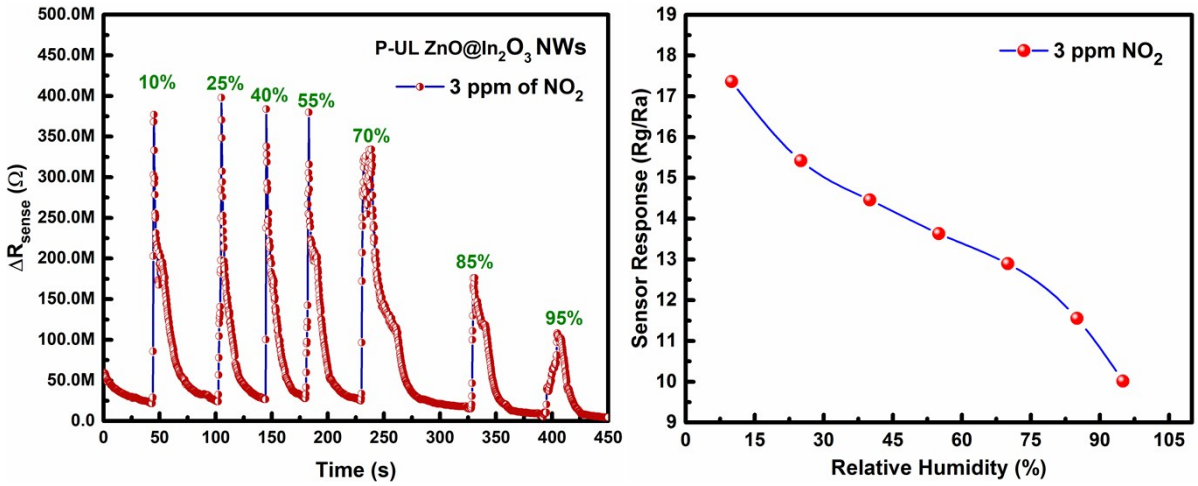

Figure S7 (a-b) Relative humidity studies of mesoporous ZnO@In_2O_3 heterojunction nanowires

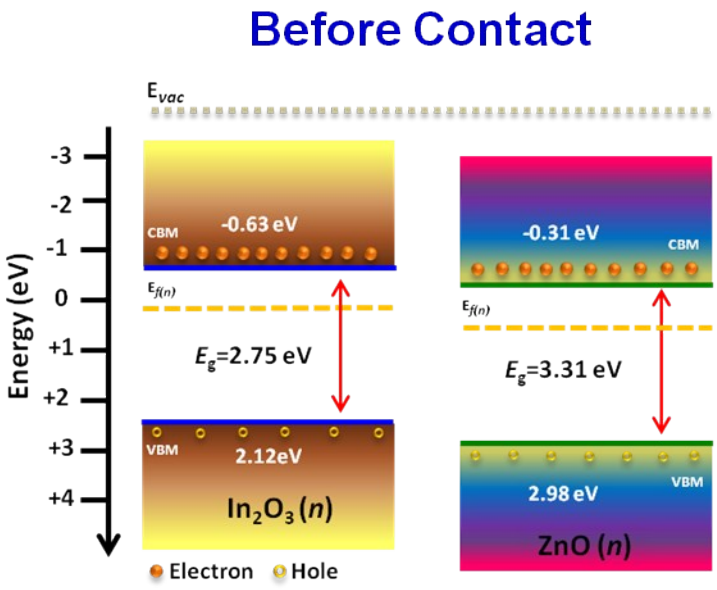

Scheme S1 Schematic energy band structure of ZnO@In_2O_3 heterojunction nanowire before contact.